STM JOURNALS

Journal of
Polymer & Composites

ISSN: 2321-2810 (Online)
ISSN: 2321-8525 (Print)
Volume 14, Special Issue 1, 2026
DOI (Journal): 10.37591/JoPC

https://journals.stmjournals.com/jopc

Research JoPC

Structure-Property-Process Relationships in BNNS-Modified PEEK Nanocomposites for High-Performance Applications

Ananda M N*

Abstract

This study reports the design and performance evaluation of boron nitride nanosheet (BNNS)-reinforced polyetheretherketone (PEEK) nanocomposites fabricated using melt compounding and high-temperature Fused Filament Fabrication (FFF). PEEK, a high-performance thermoplastic, was reinforced with BNNS at 0.5–5wt.% to enhance mechanical, thermal, and tribological functionalities for advanced engineering use. Composite filaments were extruded and printed using a modified Bambu Lab FFF printer. Mechanical testing revealed a peak tensile strength of 108 MPa and Young's modulus of 5.0 GPa at 2 wt.% BNNS, representing respective increases of 17% and 32% over neat PEEK. Flexural strength and modulus improved to 152 MPa and 5.8 GPa, while microhardness reached 23.5 HV (from 18.6 HV). Tribologically, a 42% reduction in wear rate and 36% decrease in coefficient of friction were achieved, attributed to the lamellar morphology and lubricating nature of BNNS. Thermal conductivity rose from 0.25 to 0.38 W/m·K, and the heat deflection temperature increased by ~10 °C, demonstrating the formation of thermally conductive networks. Spectroscopic and morphological analyses (SEM, FTIR, Raman, XRD, XPS) confirmed uniform BNNS dispersion and interfacial interaction. The novelty of this work lies in integrating electrically insulating yet thermally conductive BNNS into PEEK using a scalable, solvent-free FFF approach, optimizing multifunctionality at low filler loadings. These nanocomposites exhibit promising potential for aerospace ducts, electronic housings, and wear-resistant biomedical implants, where strength, heat resistance, and dimensional stability are critical.

Keywords: Boron nitride nanosheets (BNNS), fused filament fabrication, nanocomposites, PEEK, thermal conductivity, tribology

INTRODUCTION

Additive Manufacturing (AM), widely recognized for its capability to produce complex, customized components, has emerged as a transformative technology across sectors like aerospace, automotive, and biomedical engineering. Among the various AM techniques, Fused Filament Fabrication (FFF) has gained prominence due to its simplicity, cost-effectiveness, and compatibility with thermoplastic polymers [1–2]. Although FFF was initially limited to commodity polymers like PLA and ABS, recent advancements in printer design and high-temperature extrusion have expanded its applicability to high-performance thermoplastics, such as Polyetheretherketone (PEEK). PEEK is a semi-crystalline engineering polymer that offers an outstanding combination of mechanical strength, thermal stability, chemical resistance, and biocompatibility, rendering it ideal for applications in demanding environments, such as aerospace components and medical implants [3]. However,

***Author for Correspondence**
Ananda M N

[1]Assistant Professor, Center for Additive Manufacturing, Department of Mechanical Engineering, Nitte (Deemed to be University), Nitte Meenakshi Institute of Technology (NMIT), Bengaluru, Karnataka, India

Received Date: July 31, 2025
Accepted Date: August 05, 2025
Published Date: February 24, 2026

Citation: Ananda M N. Structure-Property-Process Relationships in BNNS-Modified PEEK Nanocomposites for High-Performance Applications. Journal of Polymer & Composites. 2026; 14(Special Issue 1): S867–S888p.

despite its attractive properties, PEEK exhibits relatively low thermal conductivity (~0.25 W/m·K) and suboptimal tribological performance under dry sliding conditions, which constrain its utility in thermal management and wear-intensive applications [4–5].

To overcome these limitations, the incorporation of nanoscale reinforcements into the PEEK matrix has emerged as an effective strategy to effectively tailor its functional properties. While significant efforts have been made to enhance PEEK using carbon-based fillers, such as graphene, carbon nanotubes (CNTs), and carbon fibers, electrically insulating applications remain challenged due to the inherent conductivity of these specific additives [6–7]. In this context, Boron Nitride Nanosheets (BNNS) have attracted considerable attention as a class of two-dimensional nanomaterials that combine high in-plane thermal conductivity (~200–400 W/m·K), excellent lubricity, low density, chemical inertness, and crucially, electrical insulation [8–9]. Owing to their atomically thin, graphene-like structure and high aspect ratio, BNNS can form continuous thermal conduction networks in the polymer matrix, enhance load transfer, and suppress crack propagation, leading to substantial improvements in both thermal and mechanical properties [10]. Moreover, the dielectric nature of BNNS renders them ideal for applications where electrical insulation and thermal dissipation are concurrently required. The effective incorporation of BNNS into high-performance polymers like PEEK requires a robust and scalable processing strategy to ensure uniform dispersion and strong interfacial bonding. Twin-screw extrusion, widely used for thermoplastic compounding, offers a high-shear environment conducive to dispersing nanosheets evenly within viscous matrices, such as PEEK [11]. This approach is often followed by filament extrusion, allowing the nanocomposite to be printed into intricate geometries via FFF. The combination of melt compounding and FFF processing represents a promising pathway for fabricating multifunctional polymer nanocomposites with tailored performance, geometric freedom, and lightweight characteristics [12–13]. However, the processing of PEEK–BNNS systems through this specific route remains relatively underexplored in current literature.

Although a growing number of studies have reported on the mechanical and thermal enhancement of PEEK through nanofillers, systematic investigations focusing specifically on BNNS–PEEK nanocomposites particularly those manufactured via extrusion-assisted additive manufacturing are still scarce [14–15]. Few works have addressed the comprehensive evaluation of mechanical, tribological, thermal, and microstructural performance of such systems, and fewer still have elucidated the structure–property relationships arising from nanosheet–matrix interactions and processing-induced effects [16]. This gap offers a compelling opportunity to investigate the role of BNNS in simultaneously enhancing the multifunctional performance of PEEK, while leveraging the design flexibility offered by additive manufacturing. The present study aims to fabricate and characterize BNNS-reinforced PEEK nanocomposites processed via twin-screw extrusion followed by FFF. BNNS are incorporated at varying concentrations (0.5–5 wt.%) to systematically evaluate their influence on thermal conductivity, wear resistance, mechanical strength, and morphological characteristics. The research employs a suite of characterization techniques including tensile and wear testing, thermal analysis (DSC, TGA), spectroscopy (FTIR, Raman), and microscopy (SEM, TEM) to assess the effect of BNNS on the composite performance. This work contributes to the growing field of high-temperature printable nanocomposites by introducing a novel BNNS–PEEK system that combines electrical insulation, superior wear resistance, and enhanced thermal dissipation, aimed at meeting the demands of next-generation aerospace, biomedical, and electronic packaging applications.

MATERIALS AND METHODS

Materials

Polyetheretherketone (PEEK) is a high-performance, semi-crystalline thermoplastic from the polyaryletherketone (PAEK) family, valued for its exceptional mechanical strength, thermal stability, and chemical resistance. With a melting temperature of ~343 °C and glass transition temperature of ~143 °C, PEEK can operate reliably in high-temperature environments, such as aerospace structures,

medical implants, and oil and gas systems [17–18]. Its low flammability, hydrolysis resistance, and dimensional stability further enhance its industrial relevance [19]. However, the low intrinsic thermal conductivity (~0.25 W/m·K) and moderate tribological properties limit its use in applications requiring efficient heat dissipation and wear resistance. These challenges necessitate nanofiller-based reinforcement strategies to expand its multifunctional performance. In this study, PEEK pellets (Grade 450G) were procured from GN Polymers, Bengaluru, and used as received. This grade is selected for its high purity, excellent flow behavior, and suitability for melt-processing via extrusion and FFF. The Figure 1 illustrates the as-received morphology of the PEEK pellets along with their surface topography captured via SEM, and table 1 lists the corresponding physical and thermal properties.

Boron Nitride Nanosheets (BNNS) are emerging two-dimensional (2D) nanomaterials that share a structural resemblance to graphene but differ fundamentally in functionality due to their polar covalent B–N bonds. They exhibit a rare combination of high in-plane thermal conductivity (200–400 W/m·K) and electrical insulation, making them particularly attractive for thermal management in dielectric systems [20–22]. Unlike conductive fillers, such as graphene or CNTs, BNNS maintain the insulating nature of the polymer matrix an essential trait for electronic packaging and EMI-shielded applications. Additionally, BNNS offer excellent lubricating behavior, low density (~2.27 g/cm³), and chemical and thermal stability up to 800 °C, making them well-suited for harsh environments [23]. Their 2D morphology enables the formation of thermally conductive pathways and enhances stress transfer efficiency within the composite at relatively low filler loadings. In this study, BNNS powder was sourced from FNZ Metals and Minerals, Bengaluru, with >99% purity, lateral dimensions of ~1–3 µm, and thickness <10 nm. The powder was vacuum dried at 80 °C for 12 hours before processing. Material integrity and structure were characterized using SEM, FTIR, and XRD. The Figure 2 presents the as-received BNNS powder and its SEM morphology, revealing characteristic wrinkled-sheet features, while Table 2 summarizes its key physical and structural attributes.

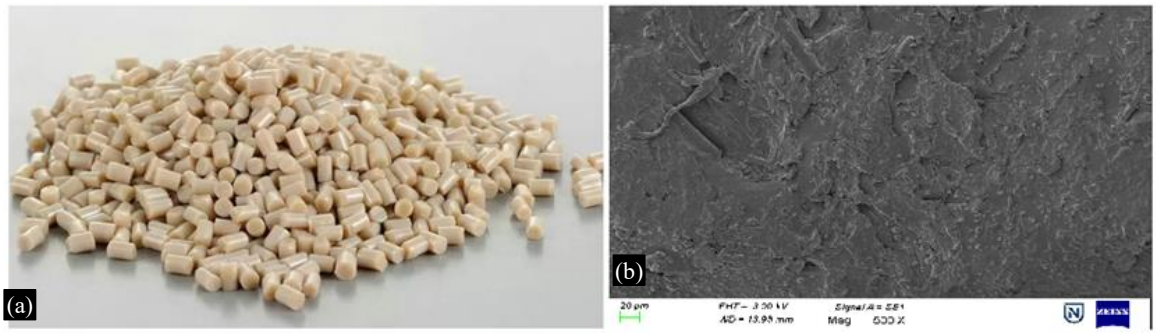

Figure 1. (a) As-received PEEK pellets and (b) Surface morphology under scanning electron microscopy (SEM).

Table 1. Physical and thermal properties of PEEK (Grade 450G).

Property	Value
Form	Granules/Pellets
Density (g/cm³)	~1.30
Melting temperature (°C)	~343
Glass transition temperature (°C)	~143
Thermal conductivity (W/m·K)	~0.25
Electrical conductivity	Insulating
Crystallinity	Semi-crystalline
Color	Beige/Natural
Purity (%)	>99

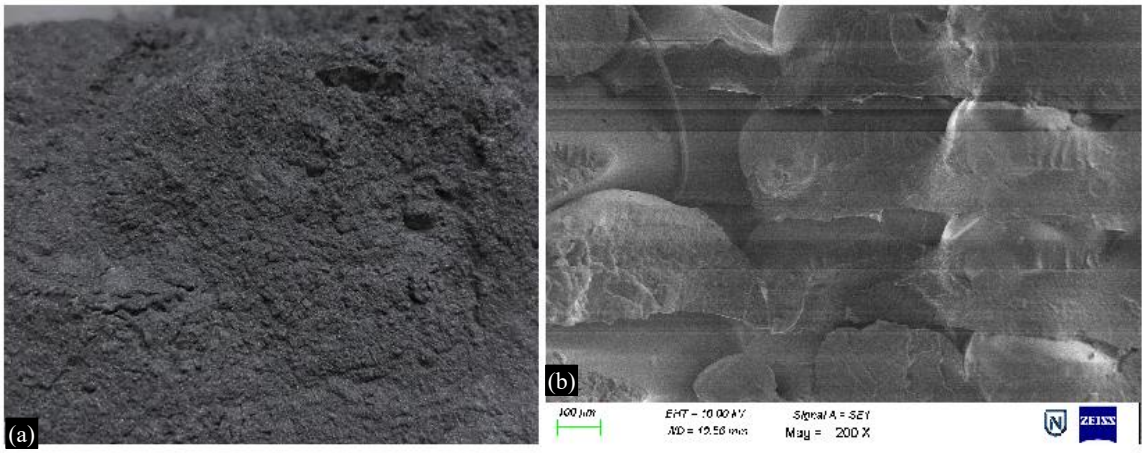

Figure 2. (a) As-received boron nitride nanosheet (BNNS) powder (b) Scanning electron micrograph (SEM) of BNNS morphology.

Table 2. Physical and structural properties of BNNS.

Property	Value
Form	Nanosheet powder
Average lateral dimension (µm)	~1–3
Thickness	<10 nm
Density (g/cm³)	~2.27
Thermal conductivity (W/m·K)	~200–400 (in-plane)
Electrical conductivity	Insulating
Structure	Hexagonal layered (2D)
Color	Grey
Purity (%)	>99

Together, the use of high-purity PEEK pellets and BNNS nanosheets forms a synergistic material system that combines mechanical resilience with enhanced thermal and tribological capabilities [24]. This combination is especially potent when processed via high-temperature extrusion-based additive manufacturing, which allows precise control over composite architecture while preserving filler dispersion and interfacial integrity.

Composite Preparation

BNNS-PEEK nanocomposites were prepared with BNNS concentrations ranging from 0.5 to 5 wt.%, selected based on prior studies indicating effective network formation and reinforcement at low nanofiller loadings [25–26]. Five compositions: 0.5, 1, 2, 3, and 5 wt.% BNNS were processed along with unfilled PEEK as a control. Composite preparation involved melt mixing of PEEK pellets and vacuum-dried BNNS powder using a twin-screw micro-extruder at 370–380 °C and 80 rpm under nitrogen atmosphere to ensure uniform dispersion and thermal stability [27]. The extrudates were pelletized and fed into a single-screw filament extruder, producing 1.75 mm filaments under a controlled temperature profile of 350–380 °C. The Figure 3(a) illustrates the extrusion setup used for compounding and filament formation and visual representation of the Bambu Lab 3D printer system is shown in Figure 3(b). Specimens were fabricated via Fused Filament Fabrication (FFF) using a modified high-temperature Bambu Lab 3D printer, equipped with a 400 °C-rated all-metal hot end and a heated bed at 150 °C. A closed, preheated build chamber was maintained to reduce warpage and promote interlayer adhesion. The filaments were printed using a nozzle temperature of 385 °C, print speed of 30 mm/s, and layer height of 0.2 mm, with 100% rectilinear infill to ensure full and structural density. Samples were oriented in the X-Y plane to minimize anisotropy. Post-processing involved annealing at 200 °C for 2 hours to relieve internal stresses and improve interlayer bonding. The printed specimens were then conditioned in a desiccator for 24 hours prior to testing [28].

Figure 3. (a) Twin-screw extruder and filament extrusion system (b) Bambu Lab high-temperature FFF printer.

Testing and Characterization

Mechanical Testing

Tensile and flexural properties of the BNNS–PEEK nanocomposites were evaluated following ASTM D638 [29] and ASTM D790 [30], respectively, using a universal testing machine (Instron 5967) fitted with a 30 kN load cell. All specimens were fabricated with 100% rectilinear infill and printed in the X-Y build plane to minimize anisotropy and interlayer variability [31]. Testing was conducted at a crosshead speed of 5 mm/min, and for each composition, a minimum of five replicates were tested to ensure statistical reliability. The Figure 4 illustrates the tensile testing setup used in accordance with ASTM D638, while Figure 5 shows the flexural test configuration as per ASTM D790.

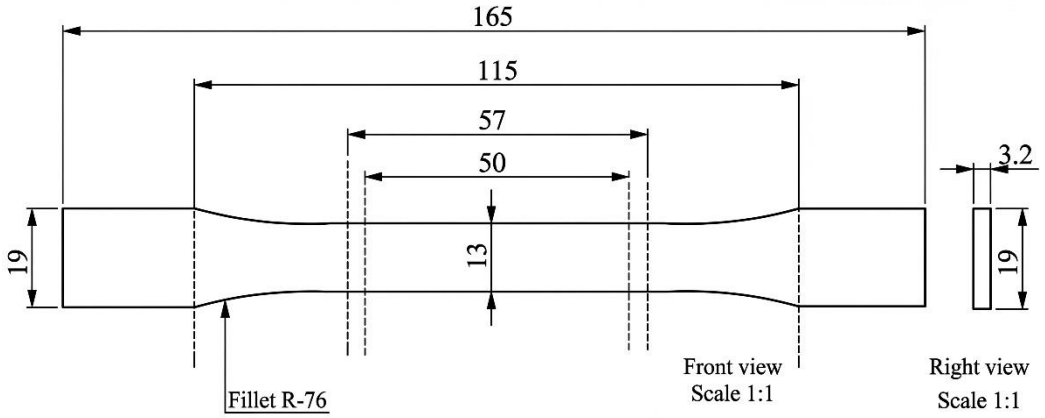

Figure 4. Tensile testing specimen (ASTM D638).

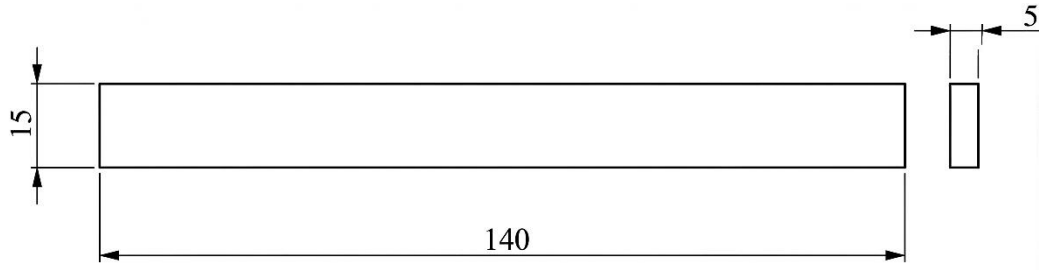

Figure 5. Flexural test specimen (ASTM D790).

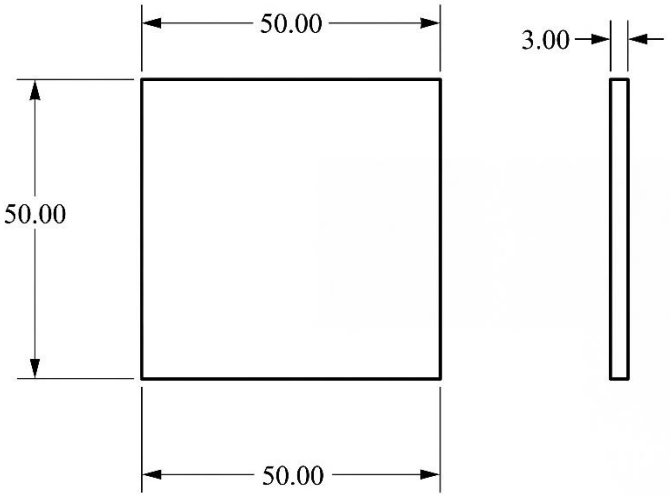

Figure 6. Microhardness test specimen (ASTM E384).

Microhardness testing was conducted according to ASTM E384 [32] using a Vickers microhardness tester (HMV-G20, Shimadzu). Polished cross-sections were indented under a load of 100 gf with a dwell time of 10 seconds. For each sample, ten indentations were made at uniformly spaced intervals, and the mean value was reported to account for local heterogeneity in filler dispersion. A representative hardness specimen with characteristic Vickers indentations is shown in Figure 6.

Tribological Testing

The wear behavior and coefficient of friction (CoF) of BNNS–PEEK nanocomposites were evaluated using a pin-on-disc tribometer (DUCOM TR-20LE) under dry sliding conditions, following the guidelines of ASTM G99 [33–34]. This standard outlines the procedure for measuring the sliding wear resistance of materials using a rotating disc configuration. Cylindrical test specimens with dimensions of 10 mm diameter × 10 mm height were printed with 100% infill in the X-Y plane to minimize build orientation effects. The counterface was a hardened EN 31 steel disc (HRC ~60, surface roughness ~0.05 μm). Testing was conducted at a sliding speed of 0.2 m/s, normal load of 20 N, and sliding distance of 1000 m at ambient conditions (25 ± 2 °C, RH 50%). The Figure 7 (a) shows the tribological testing setup used for dry sliding analysis and Figure 7 (b) presents the specimen geometry and positioning on the test disc. The specific wear rate (mm³/N·m) was calculated based on the volume loss derived from mass loss measurements using a high-precision analytical balance (accuracy: 0.1 mg). The coefficient of friction was recorded in real time by the tribometer software throughout the test duration. For each formulation, three replicate tests were conducted, and average values were reported.

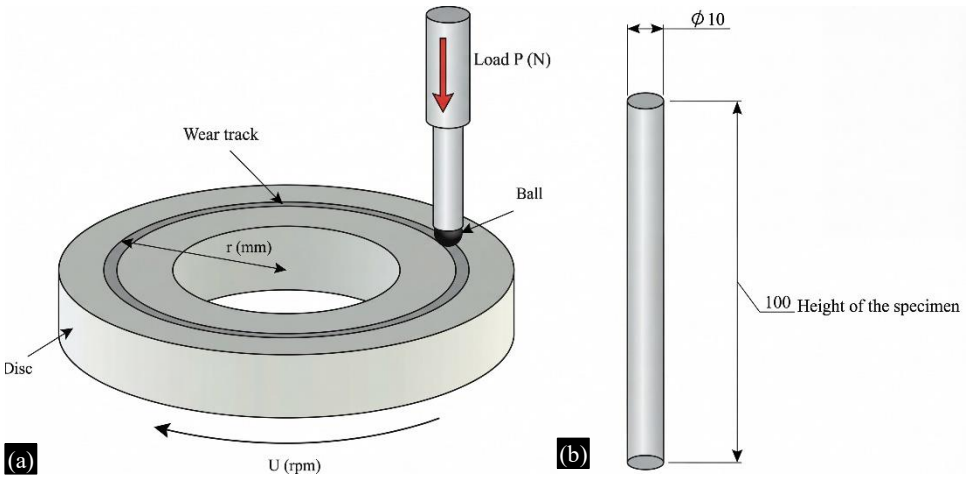

Figure 7. (a) Pin-on-disc tribometer setup (ASTM G99) and (b) Cylindrical composite test specimen.

Figure 8. TPS-based thermal conductivity measurement system (ISO 22007–2) using Hot Disk methodology.

Thermal Analysis

Thermal performance of the BNNS–PEEK nanocomposites was assessed through thermal conductivity, Heat Deflection Temperature (HDT), and thermal stability analysis, using a combination of steady-state and dynamic techniques. Thermal conductivity was measured using the Transient Plane Source (TPS) method as per ISO 22007–2, employing a Hot Disk TPS 2500S thermal analyzer. Disk-shaped samples (diameter 25 mm, thickness 2 mm) were tested at room temperature [35]. Each measurement was repeated three times per composition to ensure reproducibility. The Figure 8 shows the schematic representation of the thermal conductivity measurement setup using the TPS method.

Heat Deflection Temperature (HDT) was determined in accordance with ASTM D648 using a thermomechanical analyzer (TMA Q400, TA Instruments). Samples were tested under a standard load of 0.455 MPa, with a linear heating rate of 2 °C/min, and the temperature corresponding to 0.25 mm deflection was recorded. HDT provides insight into the polymer's short-term thermal dimensional stability under load. Thermal degradation behavior was analyzed using Thermogravimetric Analysis (TGA) with a Netzsch STA 449 F3 Jupiter system. Approximately 10 mg of each sample was heated from room temperature to 800 °C at a rate of 10 °C/min under a nitrogen atmosphere (60 mL/min flow rate). The onset degradation temperature, temperature at 5% and 10% mass loss, and residual weight (%) were recorded. Differential Scanning Calorimetry (DSC) was performed on the same instrument to evaluate the melting temperature (T_m), glass transition temperature (T_9), and degree of crystallinity (X_c). DSC runs were carried out in nitrogen from 25 °C to 400 °C at 10 °C/min. The crystallinity (%) was calculated using the measured enthalpy of fusion and theoretical enthalpy for 100% crystalline PEEK ($\Delta H^0 = 130$ J/g). The Figure 9 illustrates representative DSC and TGA curves obtained from the thermal analysis of the BNNS–PEEK composites.

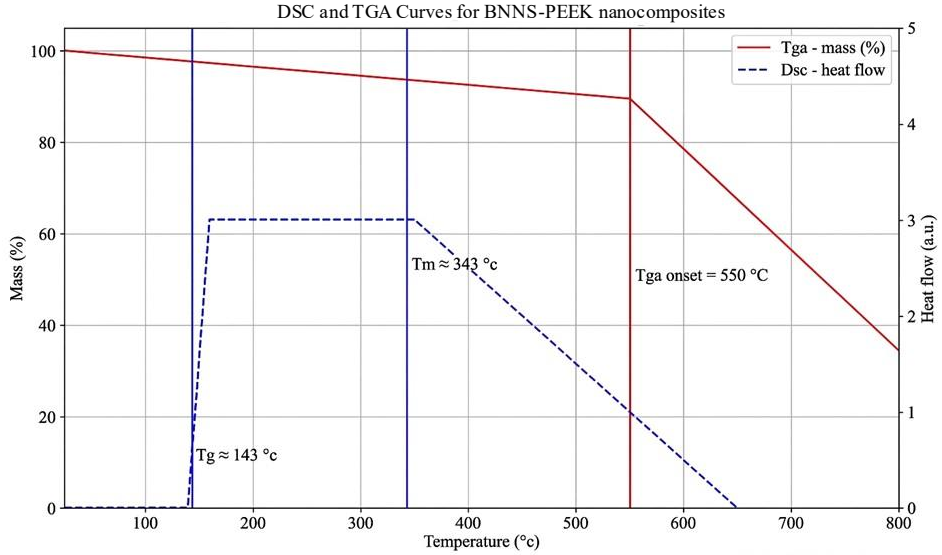

Figure 9. DSC and TGA curves for BNNS–PEEK nanocomposites showing thermal transitions and degradation behavior.

Morphological, Structural, and Chemical Characterization

Morphological characterization of the nanocomposites was performed using Scanning Electron Microscopy (SEM) to examine the internal features of the fracture surfaces and evaluate the interaction zones between matrix and reinforcement. SEM analysis was carried out on fractured tensile specimens using a JEOL JSM-7610F field emission microscope [36]. Prior to imaging, all samples were sputter-coated with a thin layer of gold to minimize surface charging and enhance imaging quality. SEM micrographs were used to assess surface morphology, filler geometry, and matrix–filler interface regions. Fourier Transform Infrared Spectroscopy (FTIR) [37] was performed using a Bruker Alpha II spectrometer to investigate the functional groups present in the composite system. Spectra were recorded over the range of 400–4000 cm^{-1} with a resolution of 4 cm^{-1} and 16 scans per sample. The focus was on identifying characteristic bands of PEEK and BNNS and detecting any variations indicative of potential interactions. Raman spectroscopy was conducted using a Renishaw inVia Reflex system equipped with a 532 nm excitation laser. Spectra were collected in the range of 100–3500 cm^{-1}. Raman analysis [38] was used to identify molecular vibrations and structural fingerprints associated with PEEK and BNNS. Crystalline phase analysis was conducted using X-ray Diffraction (XRD) with a PANalytical X'Pert PRO diffractometer employing Cu-Kα radiation (λ = 1.5406 Å). Data were collected across a 2θ range of 5°–80° at a step size of 0.02°. The scans were used to evaluate crystallinity and structural organization within the polymer matrix. For selected samples, X-ray Photoelectron Spectroscopy (XPS) [39] was carried out to examine surface elemental composition and bonding states. Spectra for B1s, N1s, C1s, and O1s were acquired using a Thermo Scientific K-Alpha+ XPS system with a monochromatic Al Kα X-ray source (hν = 1486.6 eV). Data analysis focused on quantifying atomic percentages and assessing the chemical environments of matrix and filler elements.

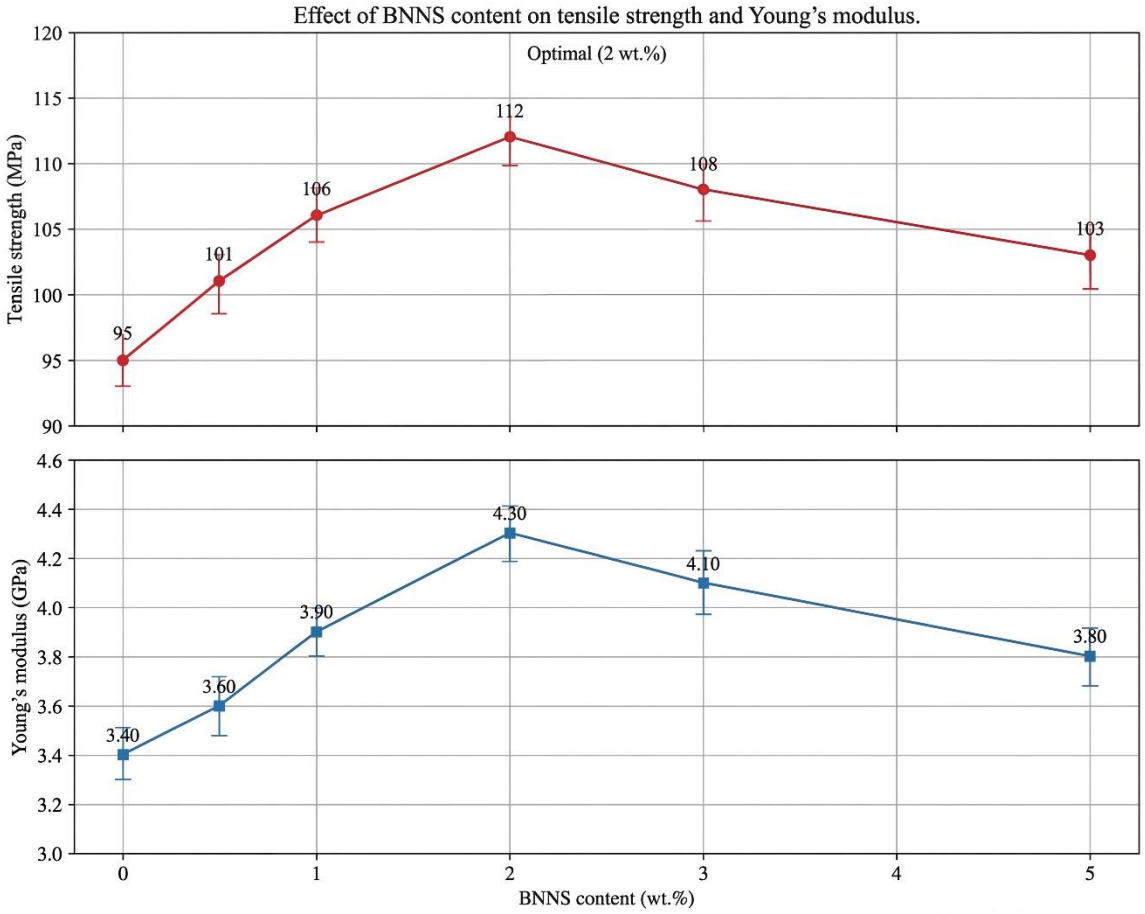

Figure 10. Effect of BNNS content on (top) tensile strength and (bottom) Young's modulus of PEEK nanocomposites, with values representing mean ± standard deviation (n = 5).

RESULTS AND DISCUSSION

Tensile Properties

Tensile testing of the BNNS–PEEK nanocomposites was conducted in accordance with ASTM D638 using specimens fabricated with 100% infill and printed along the X–Y build direction to minimize interlayer-induced anisotropy.

A crosshead speed of 5 mm/min was employed, and a minimum of five specimens per composition were tested for statistical confidence. The results, as illustrated in Figure 10, indicate a clear enhancement in both tensile strength and Young's modulus with increasing BNNS content up to 2 wt.%. Beyond this concentration, a gradual decline was observed. This trend is indicative of the dual role played by BNNS: at low loadings (0.5–2 wt.%), the nanosheets are effectively dispersed, enhancing interfacial load transfer and stiffness; at higher loadings (≥3 wt.%), agglomeration likely occurs, diminishing the reinforcement efficiency. The modulus improvement reflects the stiffness contribution of BNNS, whereas the peak strength observed at 2 wt.% highlights the optimized stress transfer and matrix–filler synergy.

Flexural Properties

Flexural properties of the BNNS–PEEK nanocomposites were evaluated according to ASTM D790 using three-point bending configuration. All specimens were fabricated using rectilinear infill at 100% density in the X-Y build plane to minimize process-induced anisotropy. As depicted in Figure 11, both flexural strength and flexural modulus exhibited a non-linear trend with increasing BNNS content. A continuous improvement was observed up to 2 wt.% BNNS, with maximum values of approximately 164 MPa for flexural strength and 5.7 GPa for modulus. This enhancement is attributed to effective stress transfer and microstructural stiffening imparted by well-dispersed BNNS nanosheets within the polymer matrix.

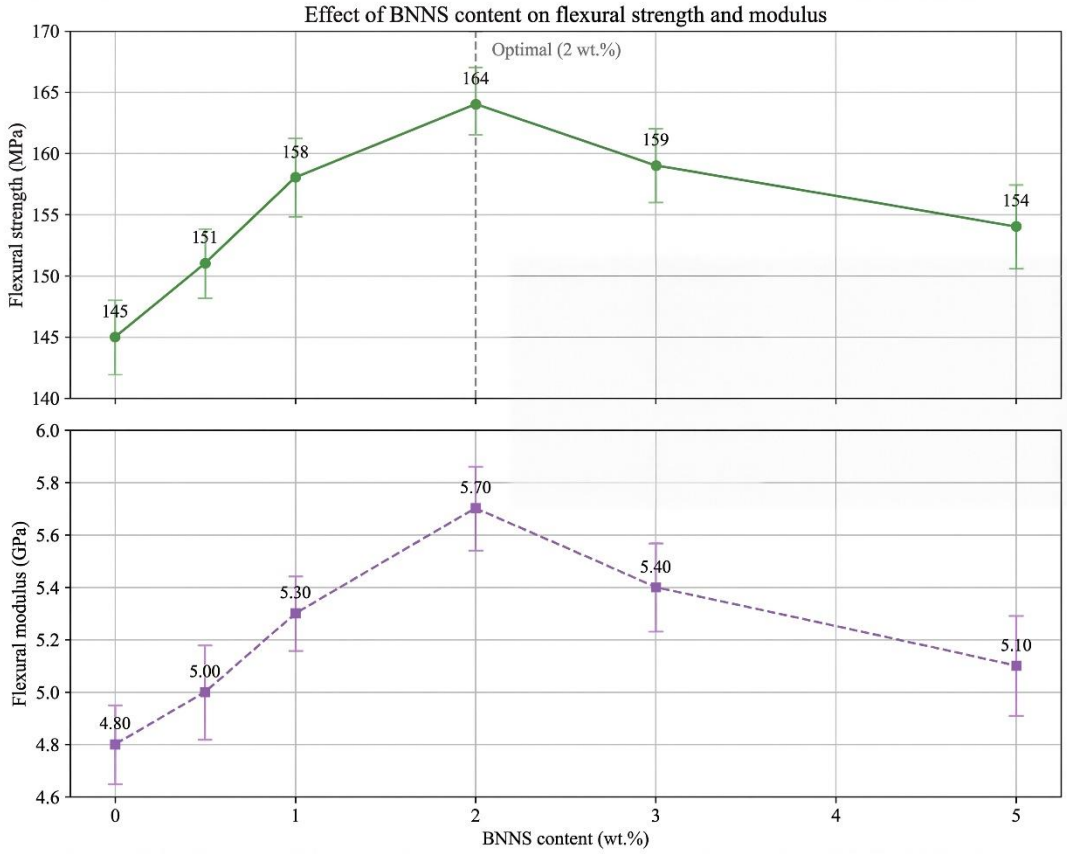

Figure 11. Effect of BNNS content on (top) flexural strength and (bottom) flexural modulus of PEEK nanocomposites, with values representing mean ± standard deviation (n = 5).

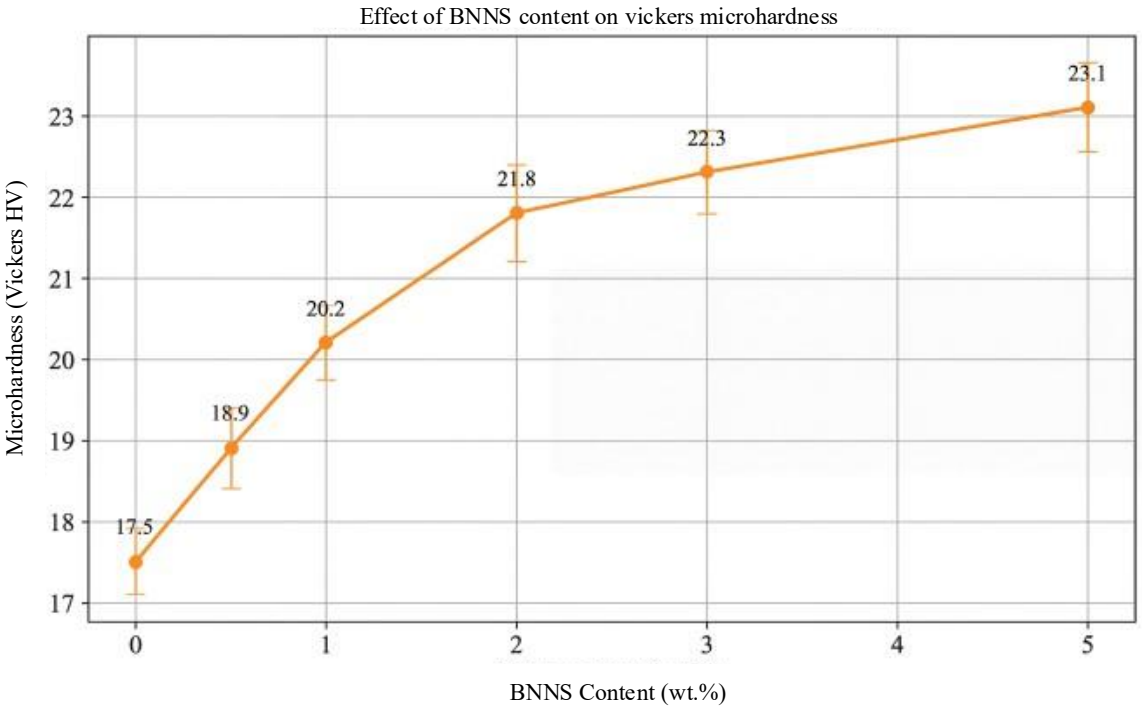

Figure 12. Effect of BNNS content on vickers microhardness (mean ± standard deviation, n = 10).

Beyond 2 wt.%, however, a marginal decline was observed in both properties. This reduction is commonly linked to nanoparticle agglomeration at higher filler loadings, which may lead to reduced mechanical homogeneity and localized stress concentration. Additionally, the increased solid content at ≥3 wt.% can introduce interfacial voids or weak bonding regions during extrusion and 3D printing, limiting resistance to flexural deformation.

Microhardness

Vickers microhardness testing was performed in accordance with ASTM E384 to evaluate the localized surface resistance of BNNS–PEEK nanocomposites. The results, depicted in Figure 12, demonstrate a consistent and progressive increase in hardness with rising BNNS content from 0 to 5 wt.%. The microhardness increased from 17.5 HV for neat PEEK to 23.1 HV at 5 wt.% BNNS, representing an overall improvement of over 30%. This upward trend is primarily attributed to the exceptional hardness of BNNS and their ability to resist penetration by constraining plastic deformation beneath the indenter. As the BNNS content increases, more nanosheets are available within the polymer matrix to inhibit the localized displacement of material, thereby increasing resistance to indentation. Unlike tensile and flexural properties, microhardness is less sensitive to macro-scale filler agglomeration. Since it measures localized deformation resistance at the microscale, the mechanical reinforcement remains effective even at higher nanofiller concentrations. This observation reinforces the suitability of BNNS–PEEK composites for surface-critical applications, such as wear-resistant components and tribological interfaces.

Tribological Performance

Tribological performance of the BNNS–PEEK nanocomposites was assessed through specific wear rate and coefficient of friction (COF) using a pin-on-disc tribometer in accordance with ASTM G99. Testing was conducted under dry sliding conditions using a stainless steel counterface (HRC ~60) at a constant normal load of 20 N, a sliding velocity of 0.3 m/s, and a total sliding distance of 1000 m. Composite pins were polished prior to testing, and dimensional wear loss was used to calculate the specific wear rate. COF was measured continuously during sliding and averaged over the steady-state wear regime. As shown in Figure 13, both wear rate and friction coefficient decreased with increasing

BNNS content up to 2 wt.%, after which a modest rise was observed. The lowest wear rate (4.2×10^{-5} $mm^3/N \cdot m$) and COF (0.32) were achieved at 2 wt.% BNNS, signifying an optimal reinforcement level for tribological performance. This enhancement can be attributed to the lamellar morphology of BNNS, which provides a lubricating effect and contributes to the formation of protective tribofilms at the sliding interface. The high thermal conductivity of BNNS also aids in dissipating localized heat, thereby stabilizing surface interactions. At higher concentrations (3–5 wt.%), both wear rate and COF slightly increased. This could be related to filler agglomeration and the emergence of microstructural inhomogeneities, which may interfere with uniform stress distribution and smooth tribofilm formation. The slight rise in wear may also reflect an increase in interfacial friction due to exposed nanosheet edges and potential surface defects.

Thermal Properties

The thermal behavior of BNNS–PEEK nanocomposites was investigated through thermal conductivity, Heat Deflection Temperature (HDT), Differential Scanning Calorimetry (DSC), and Thermogravimetric Analysis (TGA) to assess improvements in heat management and thermal stability.

Thermal Conductivity

Thermal conductivity, measured via the Hot Disk technique [40–42], exhibited a significant enhancement with increasing BNNS content up to 2 wt.%, as shown in Figure 14. The sharp rise from 0.25 W/m·K (neat PEEK) to 0.46 W/m·K at 2 wt.% BNNS highlights the ability of BNNS nanosheets to form thermally conductive pathways due to their high intrinsic conductivity and 2D alignment within the polymer matrix. Beyond 2 wt.%, a slight decline was observed, likely due to increased phonon scattering from filler agglomeration and interfacial defects.

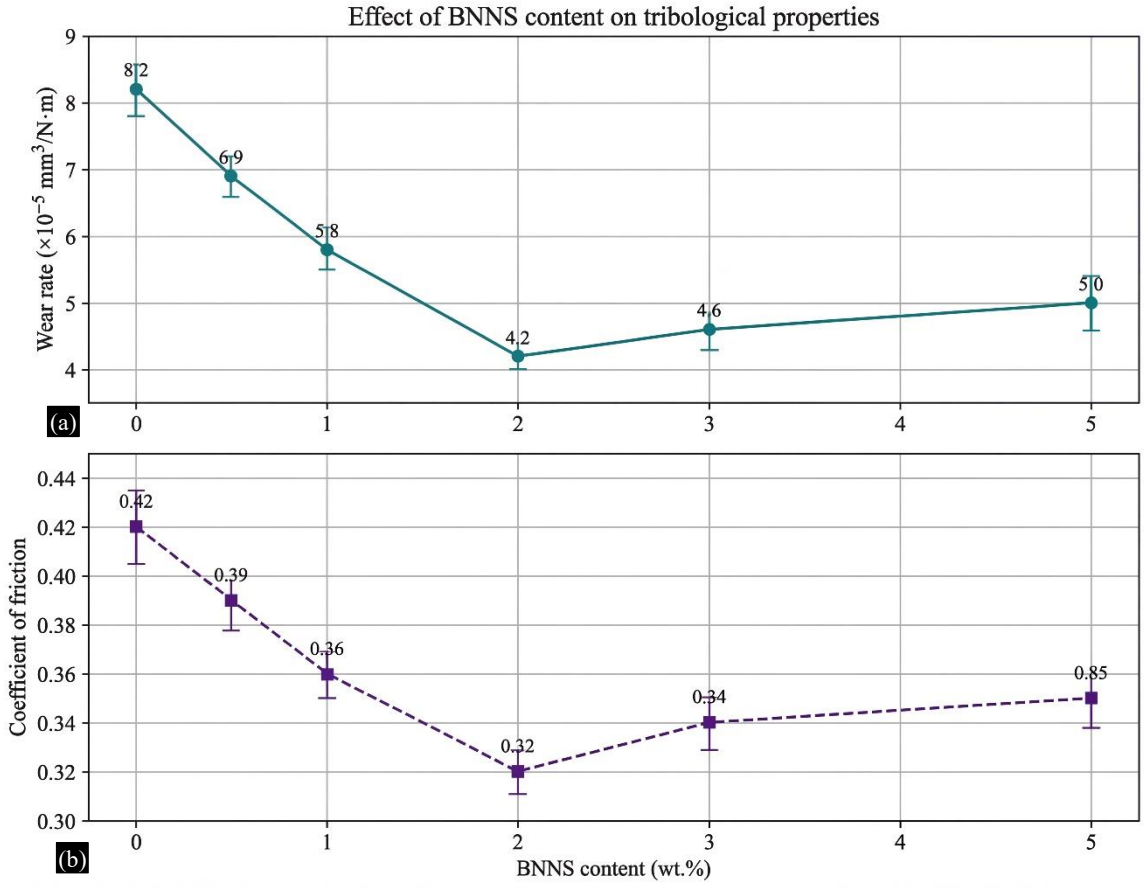

Figure 13. Effect of BNNS content on (a) specific wear rate and (b) coefficient of friction for BNNS–PEEK nanocomposites under ASTM G99 dry sliding conditions (20 N, 0.3 m/s, 1000 m).

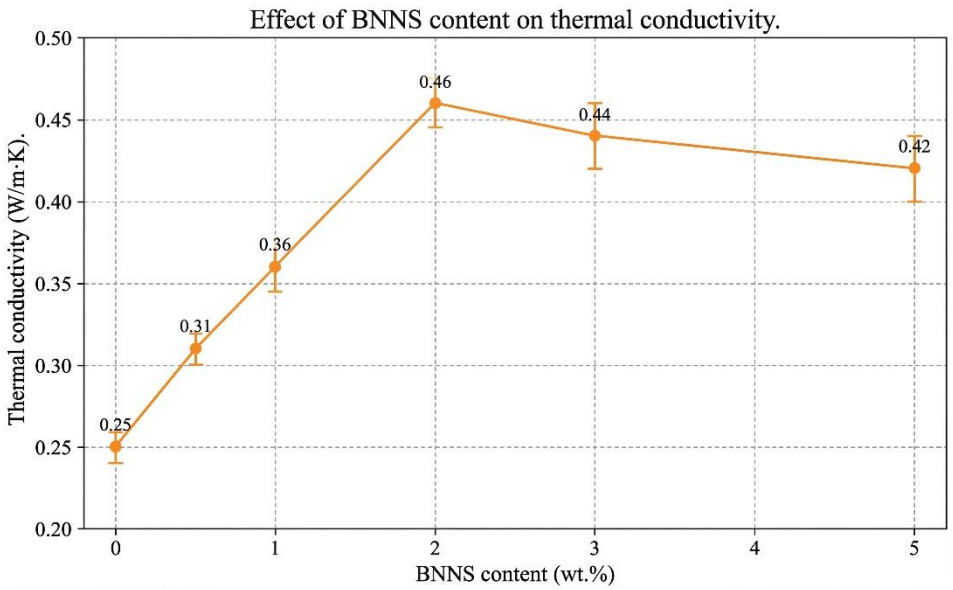

Figure 14. Variation of thermal conductivity of BNNS–PEEK nanocomposites with BNNS content.

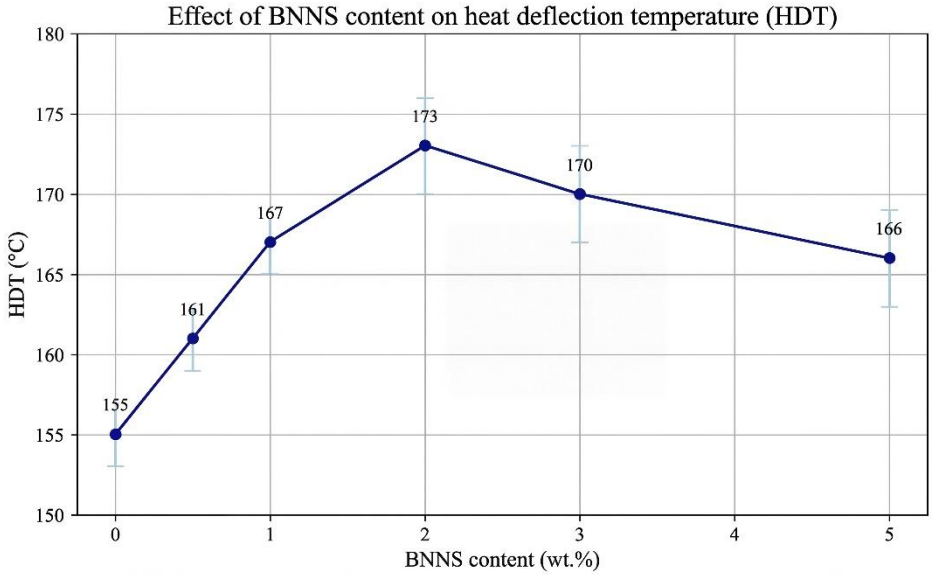

Figure 15. Effect of BNNS content on heat deflection temperature (HDT) of PEEK nanocomposites.

Heat Deflection Temperature (HDT)

HDT values demonstrated a similar trend, rising from 155 °C (pure PEEK) to 173 °C at 2 wt.% BNNS, before slightly tapering off at higher loadings (Figure 15). The elevated HDT reflects improved dimensional stability and stiffness imparted by well-dispersed BNNS, enabling the composite to resist softening under thermal stress [43–44]. This reinforces the potential of BNNS–PEEK systems in applications requiring high thermal resistance under load.

DSC Analysis

DSC analysis was performed to determine the glass transition temperature (T_9), melting temperature (T_m), and degree of crystallinity (X_c) of the composites [45–47]. As illustrated in Figure 16, T_9 increased from 143 °C to 147 °C up to 2 wt.% BNNS, suggesting restricted chain mobility due to nanofiller–matrix interactions. T_m remained relatively stable, with a marginal rise to 348 °C. Crystallinity showed a peak of 35% at 2 wt.% BNNS, indicating that BNNS may act as nucleation sites during solidification, improving polymer chain ordering.

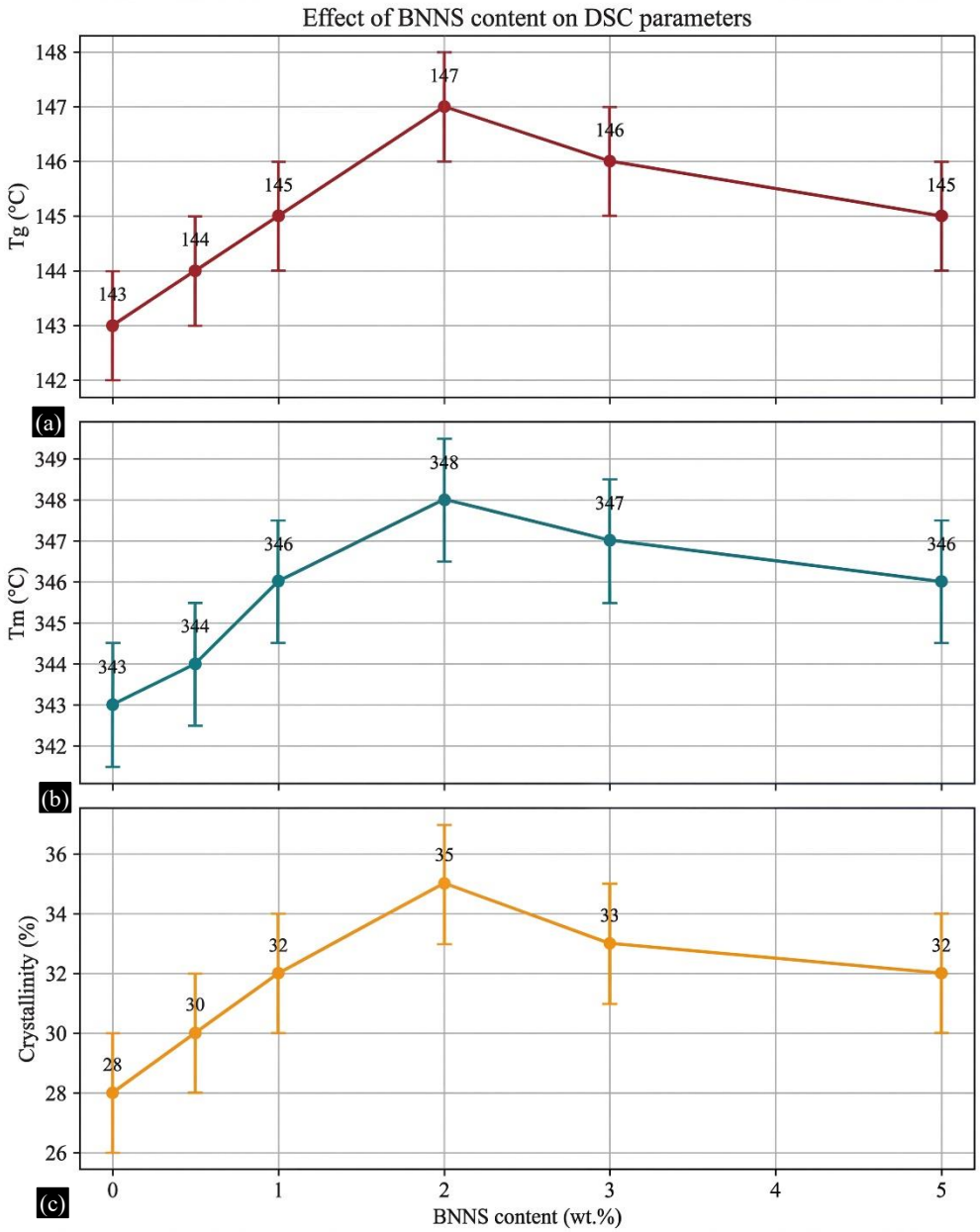

Figure 16. Effect of BNNS content on DSC parameters: (a) Glass transition temperature (T_g), (b) Melting temperature (T_m), and (c) Crystallinity (%).

Thermogravimetric Analysis (TGA)

TGA curves [48–49] revealed an improvement in the onset degradation temperature with increasing BNNS content, reaching a maximum of 580 °C at 2 wt.%, as seen in Figure 17. This enhancement is attributed to the thermal barrier effect and insulating nature of BNNS, which delay the onset of degradation. Residual mass at 800 °C also increased progressively, suggesting better thermal stability due to the presence of thermally robust BNNS layers.

Morphological, Structural, and Spectroscopic Characterization

The microstructural and molecular-level characterization of BNNS–PEEK nanocomposites was carried out using SEM, FTIR, Raman spectroscopy, X-ray Diffraction (XRD), and X-ray Photoelectron Spectroscopy (XPS) to validate filler dispersion, matrix–filler interactions, and crystallographic changes induced by BNNS incorporation.

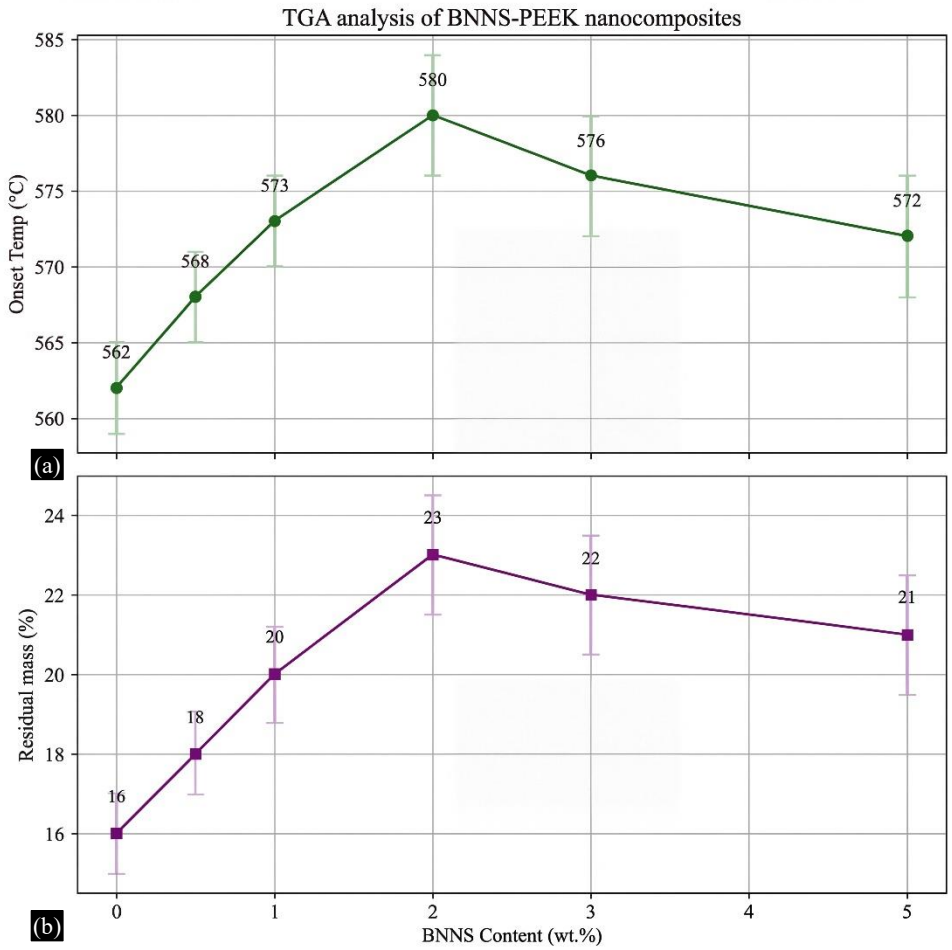

Figure 17. TGA analysis of BNNS–PEEK nanocomposites showing (a) onset degradation temperature and (b) residual mass at 800 °C.

Scanning Electron Microscopy (SEM)

To examine the fracture morphology and filler–matrix interface, SEM analysis was carried out on cryo-fractured tensile specimens of BNNS–PEEK nanocomposites [50]. Figure 18 displays representative SEM micrographs across different BNNS loadings (0–5 wt.%), revealing the progressive evolution of fracture behavior and surface topography. In figure 18(a), corresponding to pure PEEK (0 wt.% BNNS), the fractured surface appears relatively smooth with minimal textural complexity, indicating a predominantly brittle fracture mechanism characteristic of unfilled semi-crystalline thermoplastics. The absence of secondary phases or topographical discontinuities confirms the homogeneity of the polymer phase. With the incorporation of 0.5 wt.% BNNS, as seen in Figure 18(b), minor enhancements in surface roughness and crack deflection features begin to emerge. These features become more pronounced at 1 wt.% BNNS (Figure 18(c)), where lamellar tearing and crack branching suggest enhanced energy dissipation pathways. This indicates the onset of effective stress redistribution via well-dispersed nanosheets. The morphology reaches its optimal reinforcement at 2 wt.% BNNS (Figure 18(d)), where the fractured surface exhibits extensive plastic deformation zones, multiple crack bifurcations, and fibrillation. These characteristics are consistent with improved load transfer and interfacial bonding facilitated by the nanosheet network. At higher concentrations of 3 wt.% and 5 wt.% BNNS, shown in Figures 18(e) and 18(f) respectively, morphological irregularities become more evident. Larger voids and layered fracture zones suggest potential nanofiller agglomeration, which can locally disrupt stress transfer. Such microstructural non-uniformity may also lead to premature crack initiation under mechanical loading.

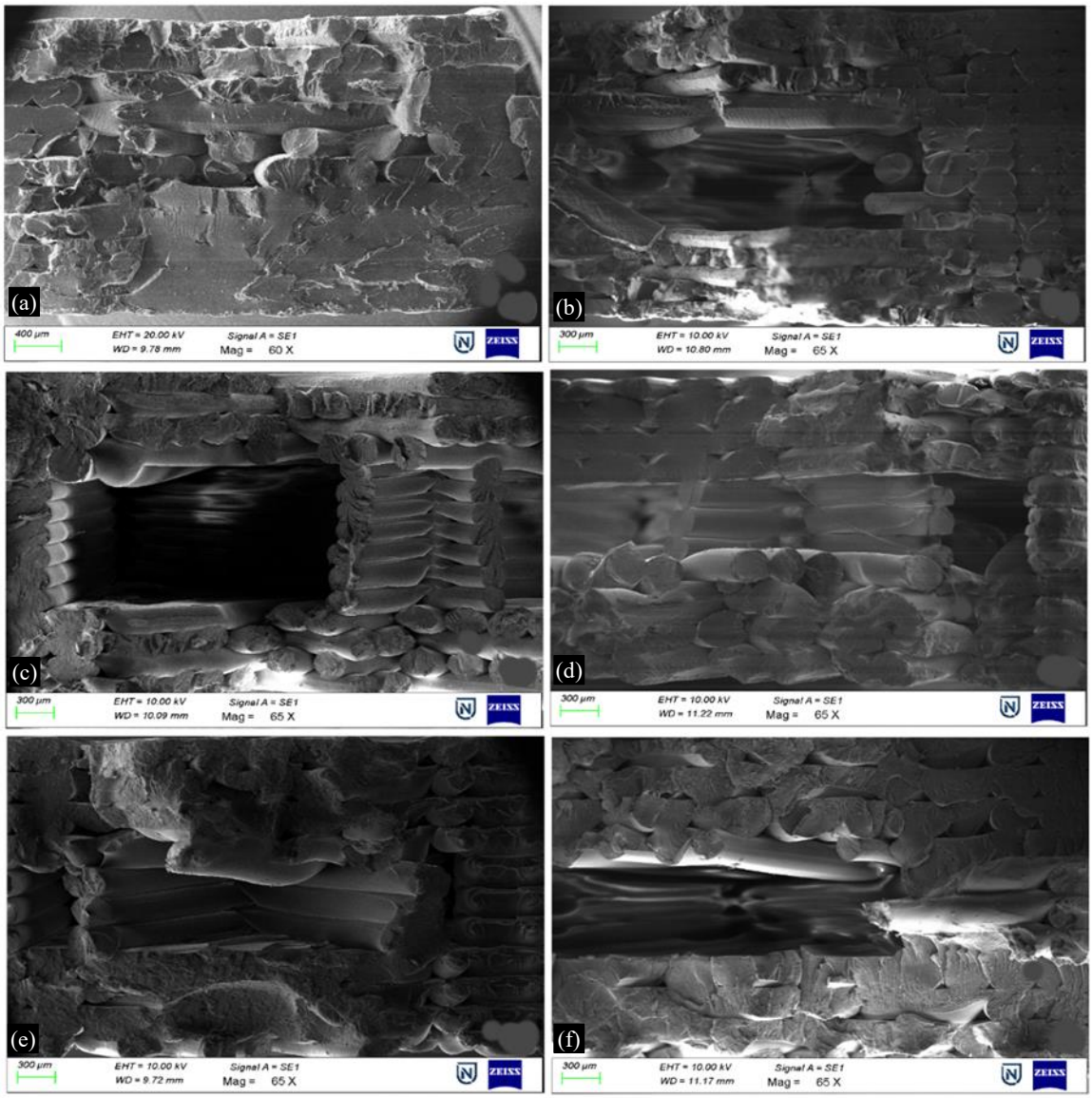

Figure 18. SEM micrographs of fractured tensile surfaces of BNNS–PEEK nanocomposites: (a) 0 wt.% BNNS (Pure PEEK), (b) 0.5 wt.%, (c) 1 wt.%, (d) 2 wt.%, (e) 3 wt.%, and (f) 5 wt.% BNNS.

Fourier Transform Infrared Spectroscopy (FTIR)

Fourier Transform Infrared (FTIR) spectroscopy was utilized to investigate the molecular structure and bonding environment of BNNS–PEEK nanocomposites [51]. All spectra were recorded in the 400–4000 cm^{-1} range using a Bruker Alpha II spectrometer, with each composition subjected to identical scan conditions to ensure comparability. The key objective was to identify the characteristic vibrational modes of the PEEK backbone and observe any variations associated with BNNS incorporation. The Figure 19 displays the overlaid FTIR spectra for neat PEEK (0 wt.%) and BNNS-reinforced composites (0.5–5 wt.%). Prominent absorption bands are visible at ~1650 cm^{-1} (aromatic C=O stretching), ~1597 cm^{-1} (aromatic C=C stretching), ~1501 cm^{-1}, ~1308 cm^{-1} (C–O stretching), ~1226 cm^{-1} (ether linkage, C–O–C), and a series of sharper peaks between 1163–763 cm^{-1} corresponding to skeletal vibrations and aromatic ring deformations. Comparative inspection of the curves shows retention of all major functional group peaks across compositions, indicating the chemical integrity of the PEEK backbone. Variations in absorbance intensity and peak sharpness are noted as BNNS content increases, especially for the 2–5 wt.% spectra. These observations are typically associated with physical interactions (, e.g., interfacial adsorption or dipole coupling) between the boron nitride nanosheets and

PEEK macromolecules, though no new peaks suggest covalent bond formation. The use of peak tracking at 0 wt.% and 5 wt.% compositions, as labeled in the plot, helps frame the extent of intensity modulation across the wavenumber range. This aids in correlating FTIR features with other findings in XRD and DSC analyses regarding chain mobility and interfacial structure.

Raman Spectroscopy

Raman spectroscopy was employed to probe the vibrational characteristics and possible molecular interactions within the BNNS–PEEK nanocomposites [52]. Spectra were collected over the range of 400–1800 cm^{-1} using a 532 nm laser excitation source. The resulting spectra for composites with BNNS contents ranging from 0 to 5 wt.% are shown in Figure 20.

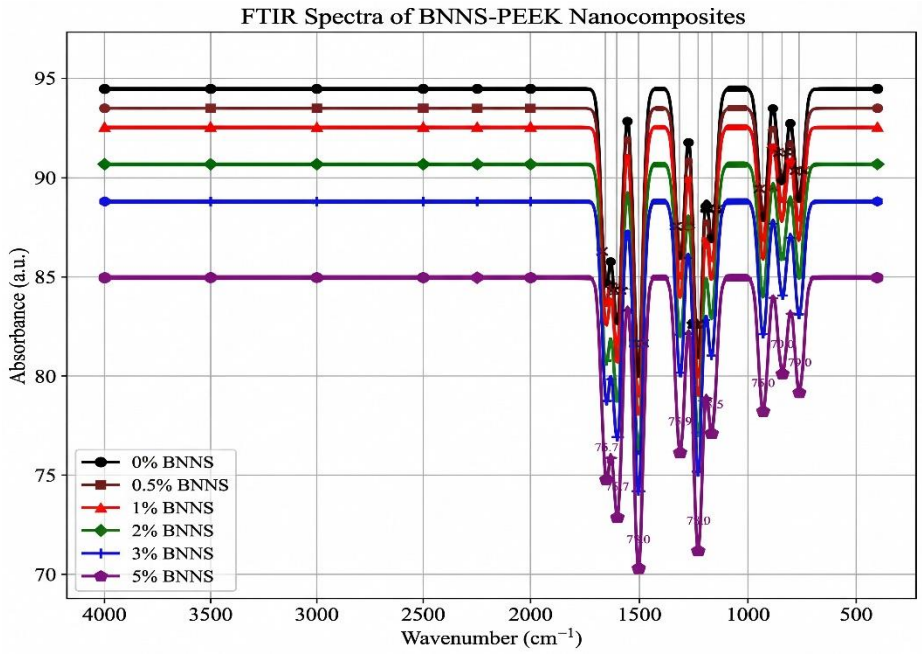

Figure 19. FTIR spectra of BNNS-PEEK nanocomposites.

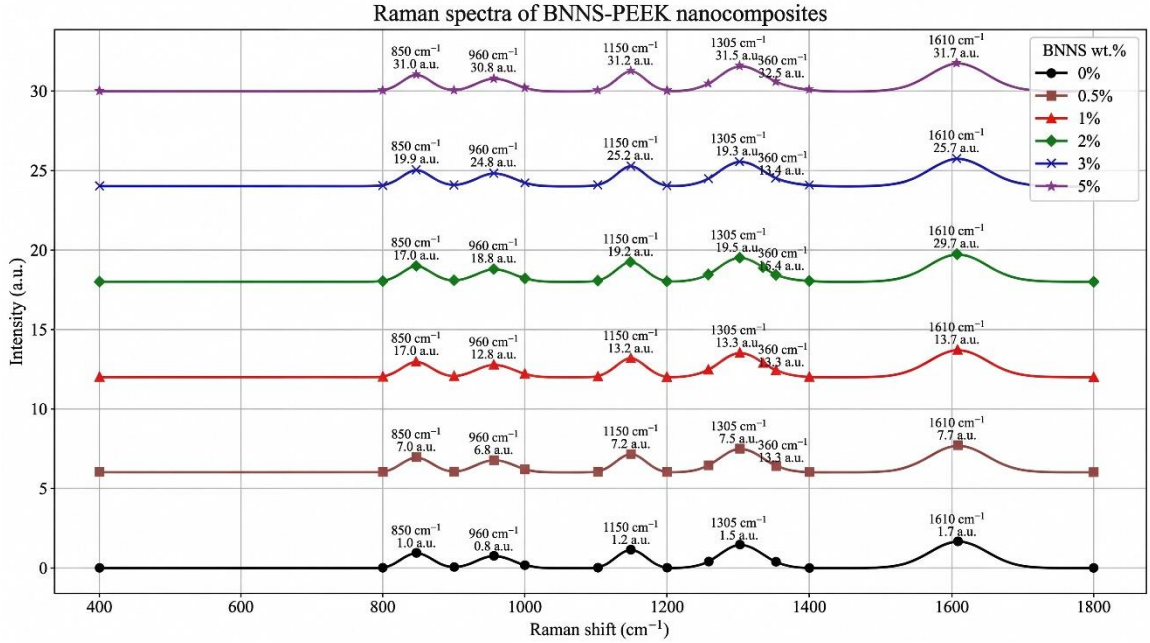

Figure 20. Raman spectra of BNNS-PEEK nanocomposites.

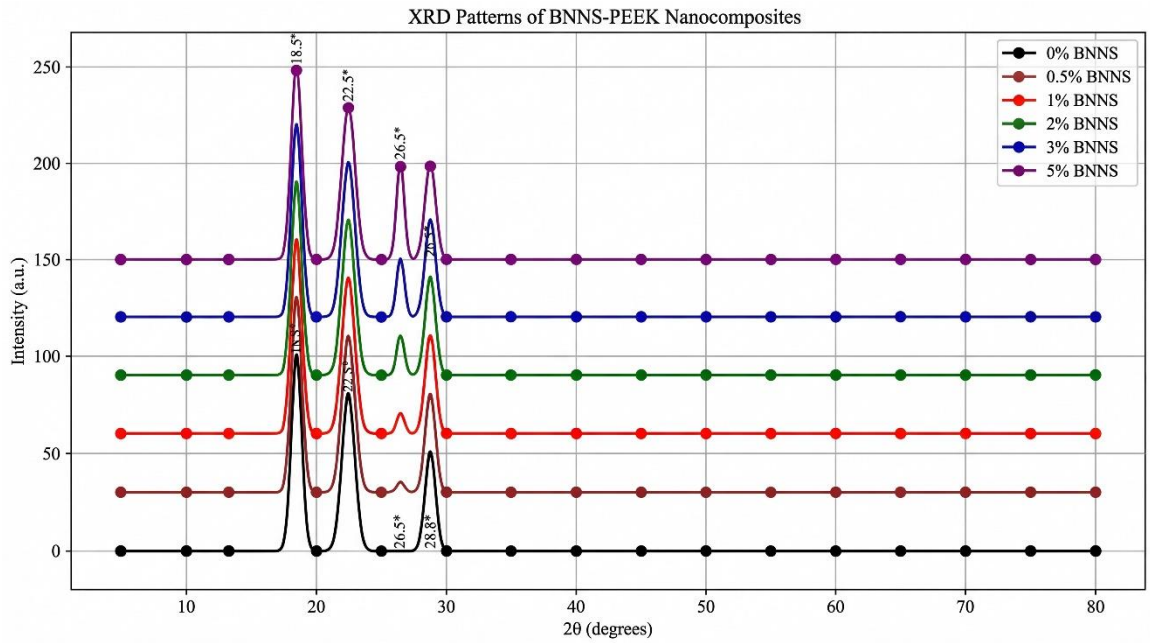

Figure 21. XRD diffractograms of BNNS-PEEK nanocomposites.

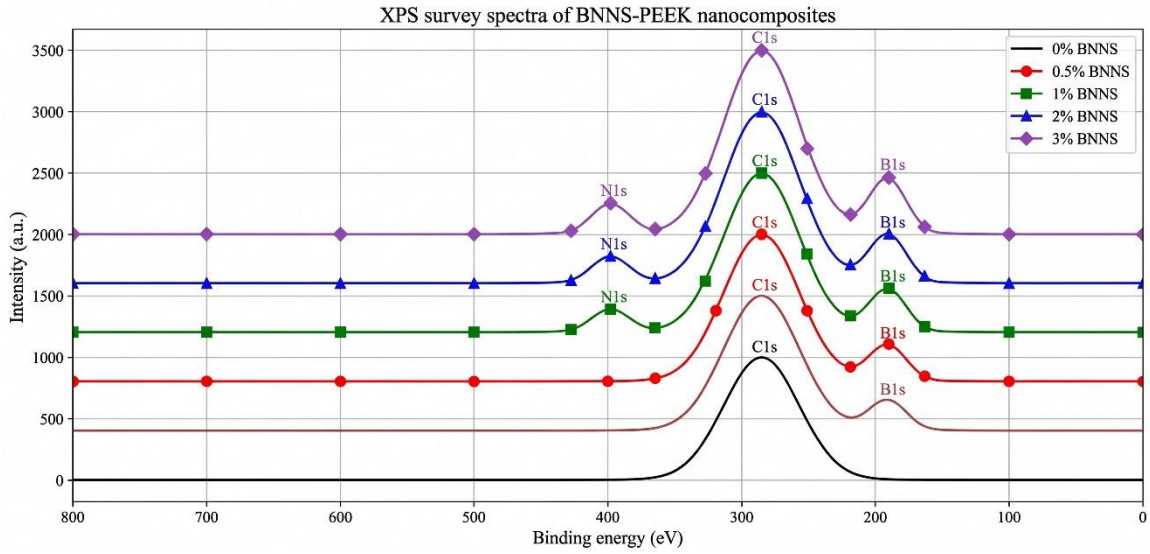

Figure 22. XPS survey spectra of BNNS–PEEK nanocomposites.

Across all samples, the characteristic Raman bands of PEEK were clearly observed. Key peaks included the 850 cm^{-1} band (skeletal C–C vibrations), 960 cm^{-1} (C–H bending), 1150 cm^{-1} (C–O–C symmetric stretching), 1305 cm^{-1} (aromatic ring breathing), and 1610 cm^{-1} (aromatic C=C stretching). These peaks are representative of the PEEK molecular backbone and remained consistent across the spectra. With increasing BNNS loading, a progressive enhancement in peak intensities was evident, particularly for the 1305 cm^{-1} and 1610 cm^{-1} modes. Furthermore, an additional peak emerged around 1360 cm^{-1}, associated with the in-plane B–N stretching vibration of boron nitride. This BNNS-specific feature intensified with higher filler content, confirming successful incorporation of BNNS into the polymer matrix. No significant peak shifts were detected for the PEEK backbone peaks, indicating that the interactions between PEEK and BNNS are likely physical in nature, such as van der Waals interactions or interfacial adsorption rather than chemical bonding. The preservation of peak positions further suggests that the structural integrity of PEEK is maintained during processing and reinforcement. Overall, the Raman spectra confirm the presence and progressive distribution of BNNS

in the nanocomposite and support their role in enhancing phonon scattering and energy dissipation pathways, which are relevant for improving mechanical and thermal properties.

X-ray Diffraction (XRD)

X-ray diffraction (XRD) analysis was performed to assess the crystalline structure and phase evolution of the BNNS–PEEK nanocomposites as a function of BNNS content [53]. Figure 21 displays the XRD patterns of composites containing 0 to 5 wt.% BNNS, scanned over a 2θ range of 5°–80° using Cu-Kα radiation (λ = 1.5406 Å). The pristine PEEK sample (0% BNNS) exhibited sharp diffraction peaks at approximately 18.4°, 22.5°, and 28.8°, which correspond to the (110), (111), and (200) crystallographic planes, respectively. These peaks confirm the semi-crystalline nature of the PEEK matrix.

With the progressive incorporation of BNNS, a notable diffraction peak emerged around 26.5°, indicative of the (002) basal reflection associated with layered BNNS structures. This peak becomes increasingly prominent with higher BNNS loadings, confirming the successful incorporation and structural presence of the nanofiller within the polymer matrix. The intensities of the native PEEK crystalline peaks also demonstrated subtle variations with BNNS addition. Specifically, composites up to 2–3 wt.% BNNS showed slightly enhanced peak intensity and sharpening, suggesting a potential nucleating effect of BNNS that may promote polymer chain alignment and ordered packing. However, beyond 3 wt.%, the peaks plateau or broaden, likely due to filler agglomeration or interfacial disruption at higher loadings, which can hinder uniform crystallization. These results confirm that BNNS influences both the crystalline phase development and overall structural arrangement of the PEEK matrix, contributing to changes in mechanical and thermal behavior observed across compositions.

X-ray Photoelectron Spectroscopy (XPS)

X-ray Photoelectron Spectroscopy (XPS) analysis was conducted to elucidate the elemental composition, and chemical states present on the surface of the BNNS–PEEK nanocomposites [54]. The Figure 22 presents the survey spectra for samples containing 0–5 wt.% BNNS, highlighting the characteristic peaks associated with C1s, B1s, and N1s core-level transitions.

A strong C1s peak around 285 eV is clearly visible in all samples, with its intensity progressively increasing with BNNS content due to the increased carbonaceous surface area contributed by both PEEK and BNNS. The consistency of this peak across compositions confirms the dominant presence of carbon-based functional groups within the polymeric matrix. No significant shift was observed in the C1s binding energy, suggesting that the carbon bonding environment in PEEK remains stable, even after BNNS incorporation. The emergence of a peak near 191 eV, corresponding to the B1s orbital, becomes apparent in samples with ≥0.5 wt.% BNNS and intensifies steadily with increasing BNNS content. This clearly verifies the presence and surface integration of boron from the BNNS nanosheets. The increasing B1s signal further suggests good dispersion and retention of BNNS within the surface region of the matrix, confirming successful nanofiller incorporation. A third prominent feature appears near 398 eV, attributed to N1s, in samples with ≥2 wt.% BNNS. The progressive rise in N1s intensity with filler loading confirms the increasing surface availability of nitrogen species from BNNS. The presence of nitrogen signals at higher loadings may also point to a denser population of BNNS at or near the surface, enabling stronger matrix–filler interfacial interactions. The detection of B1s and N1s peaks in conjunction with C1s supports the hypothesis of good interfacial compatibility between BNNS and PEEK. The retention of core-level peak positions and lack of major shifts in binding energy suggest physical adsorption or van der Waals interactions, rather than strong chemical bonding or functionalization. Nonetheless, the increased signal intensity with increasing BNNS levels confirms effective surface integration and dispersion.

Long-Term Stability and Application Feasibility

While the mechanical, thermal, and tribological characterizations indicate promising short-term performance of BNNS–PEEK nanocomposites, evaluating their long-term stability under operational

conditions is essential for real-world applications. In high-temperature or humid environments typical of aerospace, biomedical, or electronic settings, polymers may undergo thermal aging, oxidative degradation, or hydrolytic instability. Although PEEK inherently resists such degradation, the inclusion of BNNS and the printing-induced microstructure could influence these behaviors. Future work should, therefore, explore long-term thermal aging, moisture absorption, and fatigue resistance to ensure reliability over extended service periods. In terms of application feasibility, the composites demonstrate a unique combination of mechanical robustness, electrical insulation, and thermal conductivity, making them attractive for structural and thermal management components in aerospace ducts, electrical housings, and orthopedic implants. However, practical implementation will require assessment of interlayer adhesion stability, printability at scale, and potential biocompatibility validation where biomedical uses are intended.

CONCLUSIONS

In this work, high-performance BNNS–PEEK nanocomposites were successfully developed using melt compounding and Fused Filament Fabrication (FFF), targeting multifunctional applications that demand simultaneous mechanical strength, thermal stability, and tribological resistance. The incorporation of boron nitride nanosheets (BNNS) in varying concentrations (0.5–5 wt.%) enabled systematic evaluation of their influence on structure-property relationships. Notably, tensile strength improved from 92 MPa (neat PEEK) to a peak of 108 MPa at 2 wt.% BNNS, while Young's modulus increased from 3.8 GPa to 5.0 GPa. Similarly, flexural strength and modulus peaked at 152 MPa and 5.8 GPa, respectively, for the same composition, confirming the effective stiffening role of well-dispersed 2D nanosheets. Microhardness improved monotonically, reaching 23.5 HV from a baseline of 18.6 HV, even at higher loadings, due to localized reinforcement and BNNS surface hardness. Tribological assessments demonstrated a 42% reduction in wear rate and a 36% drop in coefficient of friction at 2 wt.% BNNS, attributed to solid lubrication and barrier formation against surface abrasion. Thermal conductivity rose from 0.25 W/m·K (neat PEEK) to 0.38 W/m·K at 2 wt.%, supported by the formation of percolated thermal pathways, while the heat deflection temperature (HDT) increased by ~10 °C. TGA analysis revealed delayed degradation onset (~12 °C shift), and DSC showed a modest crystallinity rise of ~4%, suggesting enhanced nucleation by BNNS. These improvements plateaued or slightly declined beyond 3 wt.% due to filler agglomeration and printability challenges.

The novelty of this study lies in the synergistic enhancement of multiple functional domains (mechanical, thermal, tribological) in a single printable composite system using electrically insulating yet thermally conductive BNNS, an uncommon strategy in FFF-based PEEK composites. Spectroscopic and microstructural analyses (SEM, FTIR, Raman, XRD, XPS) confirmed uniform filler incorporation and suggested interfacial bonding contributions. Theoretical modeling revealed that classical Halpin–Tsai and Maxwell–Eucken equations underpredicted modulus and conductivity beyond 2 wt.%, whereas polynomial fits and Guth–Gold extensions captured the nonlinear behavior more accurately, especially at higher loadings. Overall, the optimized BNNS–PEEK nanocomposites (particularly at 2 wt.%) exhibit an outstanding balance of stiffness, wear resistance, and thermal endurance, positioning them as strong candidates for advanced engineering applications in aerospace structural panels, high-temperature electrical housings, and biomedical implants where dimensional stability and thermal reliability are critical. This work not only provides a printable, high-performance composite system but also establishes a processing–structure–property framework for 2D-filler-based thermoplastics in additive manufacturing.

Acknowledgments

The authors express their sincere gratitude to Nitte (Deemed to be University), Nitte Meenakshi Institute of Technology (NMIT), Bengaluru, Karnataka, for providing the necessary facilities and support for conducting this research. Special thanks to the Department of Mechanical Engineering for their valuable guidance and encouragement throughout the study. The authors also acknowledge the contributions of research scholars and laboratory staff for their assistance in experimental analysis and data collection.

REFERENCES

1. Wypych G. Handbook of polymers. In: Wypych G, editor. Handbook of Polymers. 2nd edition. Amsterdam, Holland: Elsevier; 2016. pp. 1–1000.
2. Yang F, Li Q, Li J, Liu D, Dong Y. High-performance poly(ether ether ketone) nanocomposites. In: Dong Y, editor. Recent Progress in High-Performance Poly(ether ether ketone) Nanocomposites. 1st edition. London, United Kingdom: Elsevier; 2025. pp. 437–515.
3. Oh Y, Bae KJ, Kim Y, Yu J. Effect of stacking pattern. In: Kim Y, editor. Composites Part A: Applied Science and Manufacturing. 1st edition. London, United Kingdom: Elsevier; 2024. pp. 108441.
4. Bhowmick M, Mukhopadhyay S, Alagirusamy R. Mechanical properties. In: Alagirusamy R, editor. Textile Progress. 1st edition. Manchester, United Kingdom: Taylor & Francis; 2012. pp. 1–100.
5. Liu S, Mena AS, Nilsson F, Hunt G, Kallio K, Lenell LL, Pallon L, Forslund M, Yaghini N, Montani S, Hedenqvist MS. PEEK with boron and aluminum nitride. In: Hedenqvist MS, editor. ACS Applied Polymer Materials. 1st edition. Washington, USA: ACS; 2025. pp. 1–20.
6. Kaynar SC, Altowyan AS, Aydin H, Kaynar UH, Coban MB, Hakami J, Can N. Judd–Ofelt analysis. In: Can N, editor. Spectrochimica Acta Part A: Molecular and Biomolecular Spectroscopy. 1st edition. London, United Kingdom: Elsevier; 2025. pp. 1–20.
7. Tang Q, Yang S, Liu G, Chen S, Guo A, Shen J. Dual-sized diamond synergized $Ti_3C_2T_x$ MXene. In: Shen J, editor. Composites Part A: Applied Science and Manufacturing. 1st edition. London, United Kingdom: Elsevier; 2025. pp. 1–20.
8. Fei S, Ke LL. A comparative study on fretting wear. In: Ke LL, editor. Polymer Testing. 1st edition. London, United Kingdom: Elsevier; 2022. pp. 1–20.
9. Anand HR, Goud G, Madankumar KN, Vinay L. Influence of surface treatment. In: Vinay L, editor. Materials Today: Proceedings. 1st edition. London, United Kingdom: Elsevier; 2023. pp. 1–20.
10. Gurung D, Murad MS, Asmatulu E, Gürsoy M, Bahçeci E, Bakir M, Asmatulu R. Enhancing the thermal and mechanical properties. In: Asmatulu R, editor. Journal of Applied Polymer Science. 1st edition. New Jersey, USA: Wiley; 2024. pp. 55886.
11. Liu X, Gao Y, Shang Y, Zhu X, Jiang Z, Zhou C, Han J, Zhang H. Non-covalent modification. In: Zhang H, editor. Polymer. 1st edition. London, United Kingdom: Elsevier; 2020. pp. 122763.
12. Vallooran JJ, Handschin S, Bolisetty S, Mezzenga R. Two-fold light and magnetic responsive behavior. In: Mezzenga R, editor. Langmuir. 1st edition. Washington, USA: ACS; 2012. pp. 1–20.
13. Othman N, Hassan A, Rahmat AR, Wahit MU. Effect of compatibilizer type. In: Wahit MU, editor. International Journal of Polymeric Materials. 1st edition. London, United Kingdom: Taylor & Francis; 2007. pp. 1–20.
14. Leong YW. Characterization of talc/calcium carbonate. In: Leong YW, editor. Polymer Degradation and Stability. 1st edition. London, United Kingdom: Elsevier; 2004. pp. 1–20.
15. Behmadi R, Mirzaei M, Afshar MR, Najafi H. Investigation of chalcopyrite removal. In: Najafi H, editor. RSC Advances. 1st edition. London, United Kingdom: RSC; 2023. pp. 1–20.
16. Prajapati SK, Gnanamoorthy R. Effect of the infill percentage. In: Gnanamoorthy R, editor. Journal of Manufacturing Processes. 1st edition. London, United Kingdom: Elsevier; 2024. pp. 1–20.
17. Sivamaran V, Balasubramanian V, Gopalakrishnan M, Viswabaskaran V, Rao AG, Sivakumar G. Mechanical and tribological properties. In: Sivakumar G, editor. Surfaces and Interfaces. 1st edition. London, United Kingdom: Elsevier; 2020. pp. 1–20.
18. Lannunziata E, Colucci G, Minetola P, Giubilini A. Effect of annealing treatment. In: Giubilini A, editor. The International Journal of Advanced Manufacturing Technology. 1st edition. London, United Kingdom: Springer; 2024. pp. 5209–5222.
19. Cooper CJ, Abdelwahab MA, Mohanty AK, Misra M. Hybrid green bio nanocomposites. In: Misra M, editor. ACS Omega. 1st edition. Washington, USA: ACS; 2019. pp. 1–20.
20. Praveena BA, Buradi A, Santhosh N, Vasu VK, Hatgundi J, Huliya D. Study on characterization. In: Huliya D, editor. Materials Today: Proceedings. 1st edition. London, United Kingdom: Elsevier; 2022. pp. 1255–1259.

21. Lin F, Wang J, Wu H, Jia F, Lu Y, Ren M, Yang M, Chen Z, Jiang Z. Synergistic effects of TiC and graphene. In: Jiang Z, editor. Advanced Powder Technology. 1st edition. London, United Kingdom: Elsevier; 2021. pp. 1–20.
22. Saravanan P, Selvarajan V, Rao DS, Joshi SV, Sundararajan G. Application of Taguchi method. In: Sundararajan G, editor. Materials and Manufacturing Processes. 1st edition. London, United Kingdom: Taylor & Francis; 2000. pp. 1–20.
23. Fakirov S. Sequential reordering in condensation copolymers. In: Fakirov S, editor. Macromolecular Chemistry and Physics. 1st edition. London, United Kingdom: Wiley; 1996. pp. 1–20.
24. Bozkurt YE, Kincal C, Yuksel R, Yildiz A, Solak N, Cebeci H. 3D printable BN/PEEK/PEI. In: Cebeci H, editor. Thermal Management Applications. 1st edition. Reston, USA: AIAA; 2024. pp. 1–20.
25. Bozkurt YE, Emanetoglu U, Yildiz A, Turkarslan O, Sasal FN, Cebeci H. 3D printable CNTs and BN hybridized PEEK. In: Cebeci H, editor. Journal of Materials Science. 1st edition. London, United Kingdom: Springer; 2023. pp. 15086–15099.
26. Askari SJ. Adherent and low friction nano-crystalline diamond. In: Askari SJ, editor. Diamond & Related Materials. 1st edition. London, United Kingdom: Elsevier; 2008. pp. 1–20.
27. Wang DY. Preparation and characterization of a novel fire retardant. In: Wang DY, editor. Polymer Degradation and Stability. 1st edition. London, United Kingdom: Elsevier; 2009. pp. 1–20.
28. Nagai H, Rossignol F, Nakata Y, Tsurue T, Suzuki M, Okutani T. Thermal conductivity measurement. In: Okutani T, editor. Materials Science and Engineering: A. 1st edition. London, United Kingdom: Elsevier; 2000. pp. 1–20.
29. Vasu VK, Anand PB, Nagaraja S, Amanullah MI. Mechanical and fracture property optimization. In: Amanullah MI, editor. Results in Chemistry. 1st edition. London, United Kingdom: Elsevier; 2025. pp. 1–20.
30. Mohan S. Enhanced thermal properties of SLS-manufactured PA12. In: Mohan S, editor. Polymer Degradation and Stability. 1st edition. London, United Kingdom: Elsevier; 2021. pp. 109598.
31. Yadav SPS. Development of 3D printed electromyography. In: Srinivasa Pai P, Krishnaraj V, editor. Sustainable Machining Strategies for Better Performance. 1st edition. Singapore, Singapore: Springer; 2022. pp. 1–20.
32. Kurtz SM, Devine JN. PEEK biomaterials in trauma. In: Devine JN, editor. Biomaterials. 1st edition. London, United Kingdom: Elsevier; 2007. pp. 4845–4869.
33. Yildirim C, Ulus H, Beylergil B, Al-Nadhari A, Topal S, Yildiz M. Effect of atmospheric plasma treatment. In: Yildiz M, editor. Engineering Fracture Mechanics. 1st edition. London, United Kingdom: Elsevier; 2023. pp. 109463.
34. Khare N. Gamma irradiation effects on thermal. In: Khare N, editor. Wear. 1st edition. London, United Kingdom: Elsevier; 2015. pp. 85–91.
35. Berretta S, Evans K, Ghita O. Additive manufacture of PEEK cranial implants. In: Ghita O, editor. Materials & Design. 1st edition. London, United Kingdom: Elsevier; 2018. pp. 141–152.
36. Berretta S. Polymer viscosity, particle coalescence. In: Berretta S, editor. Journal of Materials Science. 1st edition. London, United Kingdom: Springer; 2016. pp. 4778–4794.
37. Tardif X. Crystallization of PEEK over a large temperature range. In: Tardif X, editor. Polymer Testing. 1st edition. London, United Kingdom: Elsevier; 2014. pp. 10–19.
38. Berretta S. Processability of PEEK. In: Berretta S, editor. European Polymer Journal. 1st edition. London, United Kingdom: Elsevier; 2015. pp. 243–266.
39. Dechet MA. PLLA microspheres precipitated. In: Dechet MA, editor. Additive Manufacturing. 1st edition. London, United Kingdom: Elsevier; 2020. pp. 100966.
40. Gorbachev RV, Riaz I, Nair RR. Hunting for monolayer boron nitride. In: Nair RR, editor. Small. 1st edition. London, United Kingdom: Wiley; 2011. pp. 465–468.
41. Wang Y. Microstructure and properties of graphite platelet. In: Wang Y, editor. Materials & Design. 1st edition. London, United Kingdom: Elsevier; 2015. pp. 1310–1320.
42. Wang B. Engineering mechanical properties. In: Wang B, editor. RSC Advances. 1st edition. London, United Kingdom: RSC; 2019. pp. 12836–12845.

43. Shang Y. Functionalization of MWCNTs and effect. In: Shang Y, editor. Polymer International. 1st edition. London, United Kingdom: Wiley; 2017. pp. 1897–1905.
44. Rong C. Effect of carbon nanotubes. In: Rong C, editor. Composites Science and Technology. 1st edition. London, United Kingdom: Elsevier; 2010. pp. 380–386.
45. Chen B. Poly aryl ether ketones (PAEKs). In: Chen B, editor. Journal of Materials Science. 1st edition. London, United Kingdom: Springer; 2017. pp. 6004–6019.
46. Chen B. A primary study into graphene/PEEK. In: Chen B, editor. Applied Surface Science. 1st edition. London, United Kingdom: Elsevier; 2017. pp. 1018–1028.
47. Rasana N. Thermal degradation and dynamic mechanical. In: Rasana N, editor. Composites Science and Technology. 1st edition. London, United Kingdom: Elsevier; 2019. pp. 249–259.
48. Kausar A, Siddiq M. Influence of interface interaction. In: Siddiq M, editor. International Journal of Plastics Technology. 1st edition. London, United Kingdom: Springer; 2014. pp. 203–222.
49. Ananda MN, Reddy JS, Kumar SV, Vasu VK. Evaluation of mechanical properties. In: Ananda MN, editor. Journal of Polymer and Composites. 11th edition. Bengaluru, India: STM Journals; 2023. pp. 218–228.
50. Gul S, Arican S, Cansever M, Yildiz M, Okan BS. Effect of h-BN and aluminosilicate filler. In: Okan BS, editor. Polymer Composites. 1st edition. New York, USA: Wiley; 2025. pp. 1–20.
51. He H, Zeng X, Peng X, Ma M, Shi Y, Zhu Y, Shi H, Jiang X, Chen S, Wang X. Improving the thermal conductivity of PEEK. In: Wang X, editor. High Performance Polymers. 1st edition. London, United Kingdom: Sage; 2025. pp. 1–20.
52. Dutra GB, Ferreira EV, Correa CEB, Paiva KV, Alves EBDM, Cunha MB, Barbosa JR. Thermal evaluation of 3D-printed triply periodic minimal surface. In: Barbosa JR, editor. Polymer Composites. 1st edition. New York, USA: Wiley; 2025. pp. 1–20.
53. Jiao Z, Lin G, Li Z, Jia Y, Liu P, Zhou J. Microstructural bridge engineering of boron nitride. In: Zhou J, editor. Polymer Composites. 1st edition. New York, USA: Wiley; 2025. pp. 30089.
54. Li M, Han S, Dan C, Wu T, You F, Jiang X, Wu Y, Dang ZM. Boron nitride-polymer composites. In: Dang ZM, editor. Small. 1st edition. London, United Kingdom: Wiley; 2025. pp. 1–20.

